

Article

Dehydration of Isopropanol over Silica-Supported Heteropoly Acids

 Amal Alasmari ^{1,2} , Elena F. Kozhevnikova ¹ and Ivan V. Kozhevnikov ^{1,*} 

¹ Department of Chemistry, University of Liverpool, Liverpool L69 7ZD, UK; a.a.alasmari@liverpool.ac.uk or ahassaan@kku.edu.sa (A.A.); efkozhev@liverpool.ac.uk (E.F.K.)

² Department of Chemistry, King Khalid University, Abha 61413, Saudi Arabia

* Correspondence: kozhev@liverpool.ac.uk; Tel.: +44-151-794-2938

Abstract: Dehydration of i-PrOH is used in academic research as a test reaction to probe the acid properties of solid acid catalysts. Also, it has practical importance for the utilization of surplus acetone produced by the Hock process for the combined manufacturing of phenol and acetone as well as for the production of propene from renewable resources and waste. This study demonstrates the excellent performance of polyoxometalate acid catalysts comprising silica-supported Keggin-type heteropoly acids H₃PW₁₂O₄₀ and H₄SiW₁₂O₄₀ for gas-phase i-PrOH-to-propene dehydration at ambient pressure. These catalysts show similar efficacies, giving an i-PrOH conversion and propene selectivity of 96.8 and 99.7% for 25%HPW/SiO₂ and 97.1 and 99.4% for 25%HSiW/SiO₂ in a fixed-bed reactor at 120 °C, a relevant-to-practice i-PrOH partial pressure of 15 kPa and a contact time $W/F = 27 \text{ g h mol}^{-1}$ (GHSV = 900 mL g⁻¹ h⁻¹). The catalysts are stable, resisting deactivation for at least 24 h time on stream. The HPA/SiO₂ catalysts are superior to aluminosilicate zeolites such as H-mordenite, HZSM-5 and HY for i-PrOH-to-propene dehydration in terms of i-PrOH conversion, propene selectivity and catalyst stability.

Keywords: isopropanol; dehydration; propene; polyoxometalate; heteropoly acid; zeolite



Citation: Alasmari, A.; Kozhevnikova, E.F.; Kozhevnikov, I.V. Dehydration of Isopropanol over Silica-Supported Heteropoly Acids. *Catalysts* **2024**, *14*, 51. <https://doi.org/10.3390/catal14010051>

Academic Editors: Indra Neel Pulidindi, Thirukkallam Kanthadai Varadarajan and Balasubramanian Viswanathan

Received: 13 December 2023

Revised: 3 January 2024

Accepted: 9 January 2024

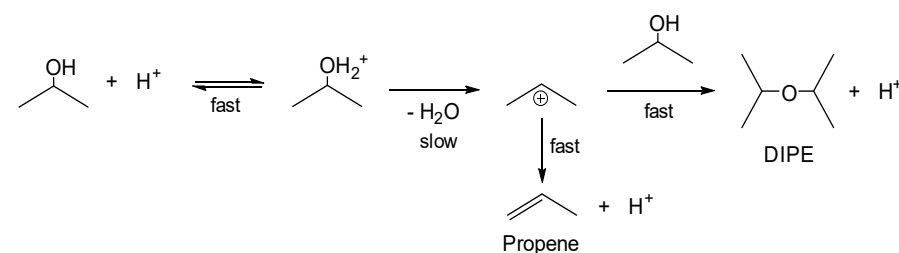
Published: 11 January 2024



Copyright: © 2024 by the authors. Licensee MDPI, Basel, Switzerland. This article is an open access article distributed under the terms and conditions of the Creative Commons Attribution (CC BY) license (<https://creativecommons.org/licenses/by/4.0/>).

1. Introduction

Dehydration of i-PrOH is widely used in academic research as a test reaction to probe the acid properties of various solid acid catalysts [1–6], including heteropoly acids (HPAs) ([2–5] and references therein). For catalysts with strong proton sites, such as HPA, i-PrOH dehydration is suggested to proceed via E1 elimination (Scheme 1) [2–4]. This mechanism involves alcohol adsorption on the Brønsted acid sites of HPA followed by C–O bond cleavage via a carbenium-ion transition state to produce isopropyl carbocation and H₂O. The carbocation forms propene through proton elimination or interacts with another alcohol molecule to give diisopropyl ether (DIPE). Via this mechanism, the reaction turnover rate scales with the HPA acid strength [3]. i-PrOH dehydration over many solid acid catalysts, including HPA, follows the Langmuir kinetics and becomes zero-order in i-PrOH at i-PrOH partial pressures above 0.6 kPa [4,6].



Scheme 1. E1 elimination mechanism for i-PrOH dehydration.

i-PrOH dehydration also has significant practical value in two regards. The first is the utilization of surplus acetone produced through the Hock process for the combined manufacturing of phenol and acetone. The second is the production of propene from renewable resources and waste. The Hock process involves the alkylation of benzene with propene to cumene, followed by cumene oxidation to cumene hydroperoxide and then acid-catalyzed cumene hydroperoxide cleavage to phenol and acetone, thus producing 0.62 tons of acetone per 1 ton of phenol [7]. This process will maintain its dominant market share as long as the coproduct acetone has a market and its surplus can be recycled back to propene. The latter is achieved through acetone hydrogenation to *i*-PrOH followed by *i*-PrOH dehydration (for a recent review, see [8]). Meanwhile, the production of propene from renewable resources and waste has been made feasible through the development of industrial-scale fermentation of abundant waste gas feedstocks, to produce acetone and isopropanol with 90% total selectivity [9]. *i*-PrOH can also be produced via biomass fermentation to an isopropanol–butanol–ethanol mixture through a modified version of the acetone–butanol–ethanol (ABE) process [10].

Industrial *i*-PrOH dehydration can be carried out under elevated or ambient pressure [8]. The process under elevated pressure is carried out at a total pressure of 20 bar and a reaction temperature of about 300 °C in the presence of γ -alumina as a catalyst. Although thermodynamically unfavorable, this process facilitates downstream separation to obtain high-purity polymer-grade propene. Meanwhile, the ambient-pressure process produces a chemical-grade propene suitable for different end users as it may contain traces of water, *i*-PrOH, DIPE, etc. For the ambient-pressure process, zeolite catalysts operating at reaction temperatures of ≤ 200 °C have been patented ([8] and references therein). Given the current global trend of sustainable economic development and minimization of the carbon footprint of the chemical industry, a more energy-efficient process for *i*-PrOH dehydration is desirable to selectively produce propene under mild conditions.

Keggin-type HPAs, also known as polyoxometalates, possess strong Brønsted acidity. These are represented by the general formula $H_{8-x}[X^{x+}M_{12}O_{40}]$, where usually $X = P^{5+}$ or Si^{4+} and $M = W^{6+}$ or Mo^{6+} [11–15]. HPAs have found several industrial applications as acid catalysts [13,15–19]. For example, silica-supported $H_4SiW_{12}O_{40}$ is used as the acid catalyst in the BP AVADA process for the production of ethyl acetate from ethene and acetic acid on a scale of >300 kt/year, which is the largest industrial application of HPA in catalysis [17–19]. Tungsten HPAs have great potential as catalysts for the ambient-pressure process of *i*-PrOH dehydration. They have very high catalytic activity in *i*-PrOH-to-propene dehydration [3–5]. However, previous studies have largely been carried out at low *i*-PrOH partial pressures ≤ 1 kPa and propene space–time yield and catalyst stability have not been optimized. Here, we investigate the gas-phase dehydration of *i*-PrOH catalyzed by silica-supported $H_3PW_{12}O_{40}$ (HPW) and $H_4SiW_{12}O_{40}$ (HSiW) at relevant-to-practice *i*-PrOH partial pressures of up to 15 kPa. The process conditions are varied to optimize isopropanol conversion, propene selectivity and catalyst stability. The HPA catalysts are compared with 10- and 12-ring aluminosilicate zeolites HZSM-5, H-mordenite and HY.

2. Results and Discussion

2.1. Catalyst Characterization

It has been shown that gas-phase dehydration of lower alcohols, such as MeOH, EtOH and *i*-PrOH, in a flow system over HPA catalysts supported on SiO_2 , TiO_2 and ZrO_2 occurs via a surface-type mechanism, with catalyst activity scaling with the number of catalyst surface proton sites [5,20]. Upon increasing HPA loading, the number of surface proton sites passes a maximum due to the decrease in catalyst surface area [5,20]. Consequently, upon increasing HPA loading, the reaction rate passes a flat maximum at between 25% and 50% HPA loading. The catalyst activity decreases in the order of $HPA/SiO_2 > HPA/TiO_2 > HPA/ZrO_2$, in line with the catalyst acid strength [5,20]. For this reason, here, we used HPA/SiO_2 catalysts with 25 and 40% HPA loading to achieve a high conversion rate of *i*-PrOH.

Information about the HPA/SiO₂ catalysts is given in Table 1. According to DRIFT spectroscopy (Figure 1), the Keggin structure of HPA in these catalysts was intact, in agreement with previous reports [5,20]. The characteristic IR bands of the Keggin polyanions [PW₁₂O₄₀]^{3−} and [SiW₁₂O₄₀]^{4−} (W=O, corner-sharing W–O–W and edge-sharing W–O–W bands) [21] could be seen in the spectra, except for the P–O band of [PW₁₂O₄₀]^{3−} at 1080 cm^{−1} and the Si–O band of [SiW₁₂O₄₀]^{4−} at 1019 cm^{−1}, which were obscured by the intense band of SiO₂ at around 1100 cm^{−1}.

Table 1. Information about HPA/SiO₂ catalysts.

Catalyst	$S_{\text{BET}}^{\text{a}}$ m ² g ^{−1}	V_{p}^{b} cm ³ g ^{−1}	D_{p}^{c} Å	Weight Loss (wt%)		$-\Delta H^{\text{d}}$ kJ mol ^{−1}	B^{e} mmol g ^{−1}
				RT–300 °C	300–700 °C		
Aerosil 300 SiO ₂	293	1.26	172	3.64	0.91		
25%HPW/SiO ₂	183	0.73	161	4.77	1.78	171	0.26
25%HSiW/SiO ₂	195	0.81	167	5.39	2.27	154	0.35
40%HPW/SiO ₂	139	0.66	191	4.36	1.31	177	0.42
40%HSiW/SiO ₂	130	0.56	172	4.79	1.52	158	0.56

^a BET surface area; the catalysts were pretreated at 220 °C in a vacuum. ^b Single-point total pore volume (at $P/P_0 = 0.99$). ^c Average pore diameter ($4V_{\text{p}}/S_{\text{BET}}$). ^d Initial enthalpy of ammonia adsorption at 150 °C (± 6 kJ mol^{−1}) [20]. ^e Total number of Brønsted acid sites per 1 g of catalyst.

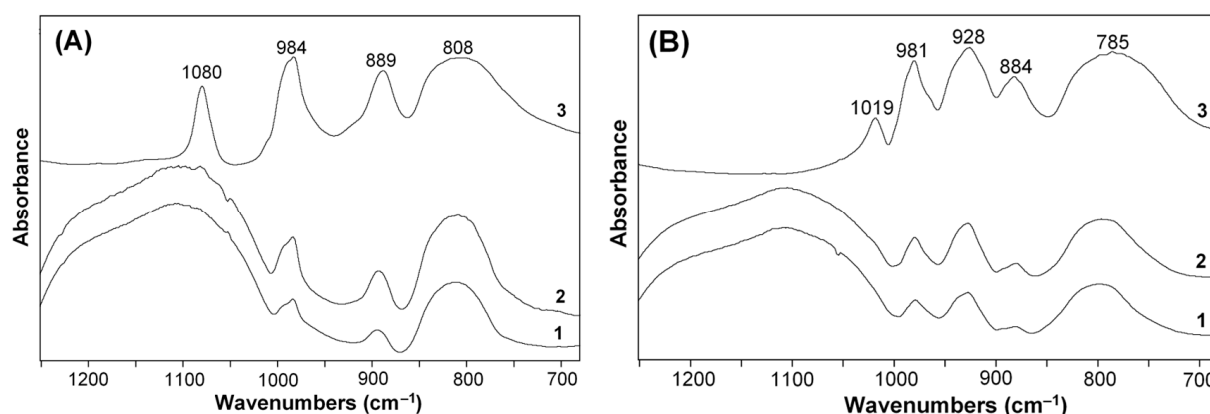


Figure 1. DRIFT spectra of bulk and supported HPA. (A): (1) 25%HPW/SiO₂, (2) 40%HPW/SiO₂, (3) bulk HPW. (B): (1) 25%HSiW/SiO₂, (2) 40%HSiW/SiO₂, (3) bulk HSiW.

XRD showed the presence of the HPA crystal phase in the HPA/SiO₂ catalysts (Figure 2), with the same XRD patterns as for the bulk HPAs. Significant line broadening indicated a higher dispersion of HPA in HPA/SiO₂ catalysts compared to bulk HPA. As estimated from the Scherrer equation, HPA particle size in the HPA/SiO₂ catalysts was 11–18 nm while that in bulk HPA was 40–60 nm. This agreed with the previous report [20]. As revealed by XRD [20], HSiW forms smaller particles on the SiO₂ surface than HPW. Hence, in HPA/SiO₂ catalysts at the same HPA loading, HSiW has a larger number of surface proton sites (proton site density) than HPW because HSiW has more protons per molecule than HPW as well as a higher dispersion on the silica surface. This could lead to greater activity of HSiW/SiO₂ catalysts per HPA weight compared to HPW/SiO₂ despite HPW having stronger acid sites than HSiW [5,20].

Bulk tungsten HPAs are known to be purely Brønsted acids, as demonstrated by IR spectroscopy of adsorbed pyridine (Py-DRIFTS) [11–14]. The Py-DRIFT spectra for bulk and silica-supported HPW and HsiW are shown in Figure 3. The bulk HPAs have solely Brønsted (B) acid sites. This is supported by the presence of the strong band of the pyridinium ion at 1540 cm^{−1}, whereas the band at 1450 cm^{−1} characteristic of Lewis (L) acid sites [22] is absent. On the contrary, SiO₂ exhibits only L sites, with no B sites capable of protonating pyridine; the L sites can be attributed to low-coordinate surface Si⁴⁺ ions.

As can be seen, the HPA/SiO₂ catalysts possess both B and L sites, with B sites by far dominating. The total number of proton sites in HPA/SiO₂ catalysts is given in Table 1.

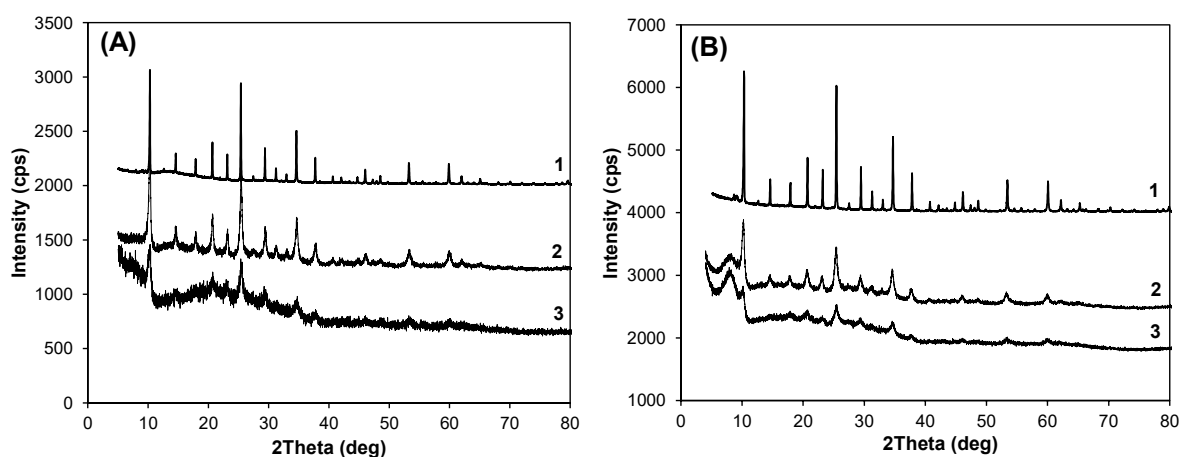


Figure 2. XRD patterns for bulk and supported HPA. (A): (1) 25%HPW/SiO₂, (2) 40%HPW/SiO₂, (3) bulk HPW. (B): (1) 25%HsiW/SiO₂, (2) 40%HsiW/SiO₂, (3) bulk HsiW.

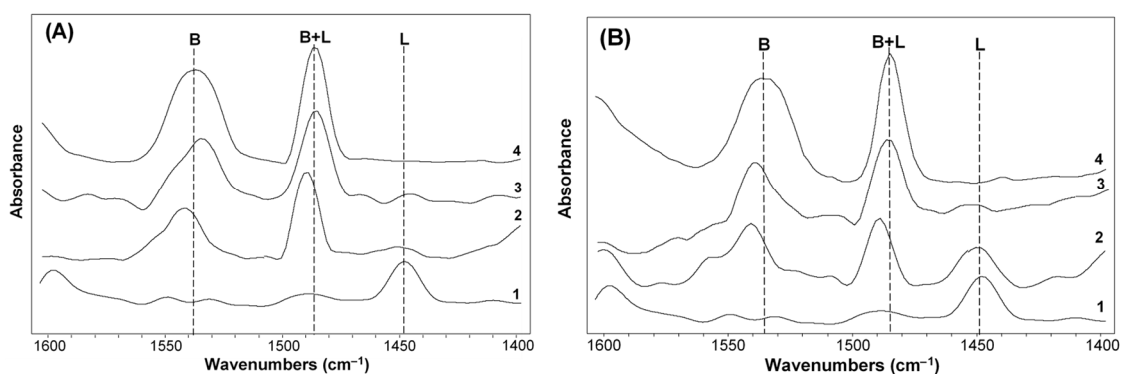


Figure 3. Py-DRIFTS for HPA catalysts. (A): (1) SiO₂, (2) 25%HPW/SiO₂, (3) 40%HPW/SiO₂, (4) bulk HPW. (B): (1) SiO₂, (2) 25%HsiW/SiO₂, (3) 40%HsiW/SiO₂, (4) bulk HsiW.

The strength of acid sites in HPA/SiO₂ catalysts has been measured using ammonia adsorption calorimetry in many previous studies [3,5,20,23–26]. This is the most accurate technique for characterizing the acid strength of HPA catalysts. Table 1 presents the values of initial enthalpy of ammonia adsorption (ΔH) for the HPA/SiO₂ catalysts under study, taken from a recent report [20]. The ΔH values are in the range of -154 to -177 kJ mol⁻¹ and characterize the strongest proton sites in these catalysts. In comparison, HZSM-5, HY and H-mordenite zeolites have weaker proton sites with ΔH values of -120 to -150 kJ mol⁻¹ [26,27].

Through TGA, we determined that HPA/SiO₂ catalysts after pretreatment at 150 °C/1 Pa retained 4–7% of the physically and chemically bound water, which was lost on heating to 700 °C, mostly from room temperature to 300 °C (Table 1).

2.2. Dehydration of Isopropanol over HPA/SiO₂ Catalysts

2.2.1. Effect of Temperature

The effect of reaction temperature on HPA-catalyzed dehydration of *i*-PrOH was studied in the temperature range of 50–100 °C at an *i*-PrOH partial pressure of 0.95 kPa, a contact time $W/F = 422$ g h mol⁻¹ and a time on stream (TOS) of 2 h. As expected, *i*-PrOH conversion increased with increasing temperature, as illustrated by the data in

Figures 4 and 5. Thus, for the 25%HSiW/SiO₂ catalyst, the conversion was 22% at 60 °C, progressing to complete conversion of ~100% at 90 °C (Figure 4). Similar results were obtained for the catalysts with 40% HPA loading (Figure 5). The selectivity to propene increased with increasing reaction temperature along with i-PrOH conversion, reaching ~100% at 90 °C. In contrast, the selectivity to diisopropyl ether (DIPE) declined to almost zero as the temperature was increased from 60 to 90 °C (Figures 4 and 5).

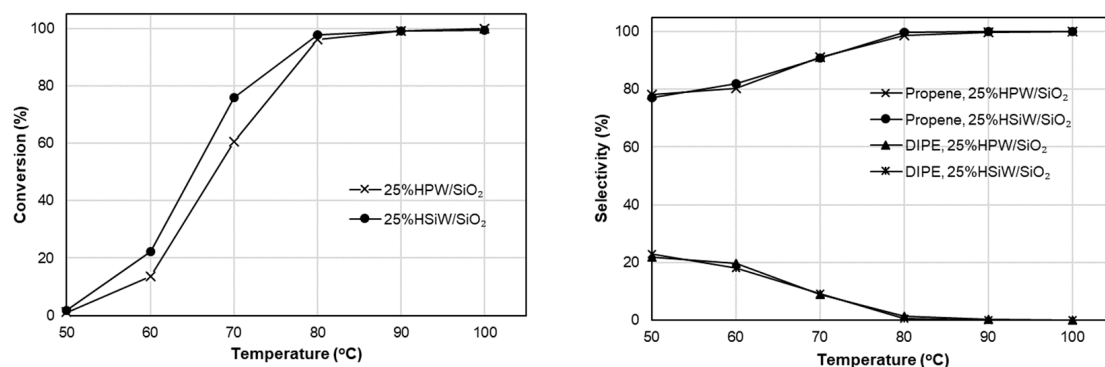


Figure 4. Effect of temperature on i-PrOH conversion and product selectivity over 25%HPW/SiO₂ and 25%HSiW/SiO₂ catalysts (0.20 g) at 20 mL min⁻¹ flow rate, 0.95 kPa i-PrOH partial pressure, W/F = 422 g h mol⁻¹ and 2 h TOS.

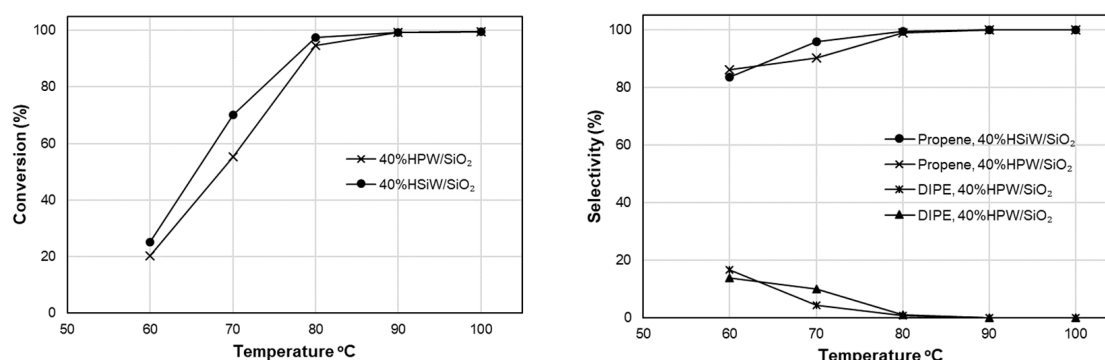


Figure 5. Effect of temperature on i-PrOH conversion and product selectivity over 40%HPW/SiO₂ and 40%HSiW/SiO₂ catalysts (0.20 g) at 20 mL min⁻¹ flow rate, 0.95 kPa i-PrOH partial pressure, W/F = 422 g h mol⁻¹ and 2 h TOS.

The results obtained demonstrated that catalysts with 25% and 40% HPA loading exhibited similar performance levels in i-PrOH dehydration. Therefore, further catalyst testing was carried out on 25%HPW/SiO₂ and 25%HSiW/SiO₂ catalysts. Before further optimizing the performance of HPA catalysts, we investigated the performance levels of several aluminosilicate zeolites in i-PrOH dehydration in order to compare the activity and selectivity of the two types of catalysts.

2.2.2. Dehydration of i-PrOH Catalyzed by Zeolites

The zeolites studied included 10-ring HZSM-5 and 12-ring HY and H-mordenite, namely, HZSM-5 (Si/Al = 12 and 20), HY (Si/Al = 18) and H-mordenite (Si/Al = 12). Zeolite texture and proton site density are shown in Table 2 and XRD patterns in Figure 6. XRD confirmed the structure and high crystallinity of the zeolite samples used.

Table 2. Zeolite catalysts.

Catalyst	$S_{\text{BET}}^{\text{a}}$ $\text{m}^2 \text{g}^{-1}$	V_{p}^{b} $\text{cm}^3 \text{g}^{-1}$	D_{p}^{c} \AA	Particle Size ^d nm	Proton Site Density ^e mmol g^{-1}
HZSM-5 (Si/Al = 12)	378	0.22	24	54	1.28
HZSM-5 (Si/Al = 20)	361	0.17	19	110	0.83
HY (Si/Al = 18)	733	0.48	26	83	0.92
H-mordenite (Si/Al = 12)	461	0.27	24	64	1.28

^a BET surface area; the catalysts were pretreated at 245 °C in a vacuum. ^b Single-point total pore volume (at $P/P_0 = 0.99$). ^c Average BET pore diameter. ^d Calculated from Scherrer equation. ^e Calculated from Si/Al ratio.

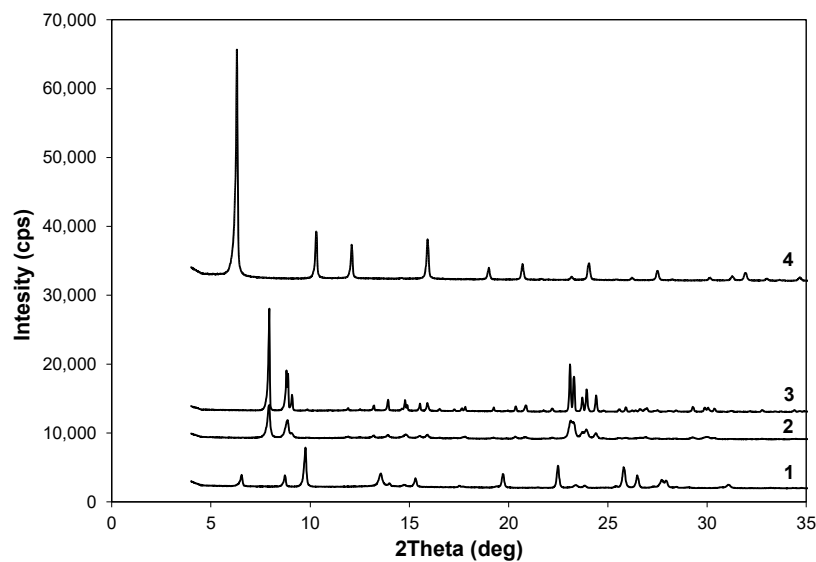


Figure 6. XRD pattern of zeolite catalysts: H-mordenite (Si/Al = 12) (1), HZSM-5 (Si/Al = 12) (2), HZSM-5 (Si/Al = 20) (3) and HY (Si/Al = 18) (4).

To draw a comparison between HPA and zeolite catalysts, the dehydration of *i*-PrOH over zeolites was studied under the same conditions as the reaction with HPA. The effect of reaction temperature on zeolite performance is illustrated by the data in Figures 7 and 8. It can be seen that under the specified reaction conditions, zeolites reached ~100% *i*-PrOH conversion and 97–100% propene selectivity at 140–180 °C. The activity of zeolites in terms of *i*-PrOH conversion was in line with their proton site density (Table 2), decreasing with an increase in the Si/Al ratio: H-mordenite (Si/Al = 12) > HZSM-5 (Si/Al = 12) > HY (Si/Al = 18) > HZSM-5 (Si/Al = 20), with the light-off temperatures of 90, 107, 115 and 140 °C corresponding to 50% *i*-PrOH conversion (Figure 7). H-mordenite showed a better performance, which can be attributed to the favorable combination of its stronger acidity [27], large pore size and large proton site density. The low activity of HZSM-5 (Si/Al = 20) may have been caused by its smaller proton site density as well as by its larger particle size (Table 2) impeding access to the acid sites inside micropores.

Figure 7 compares the data for the zeolites and 25%HPA/SiO₂ catalysts, clearly demonstrating much greater activity of HPA catalysts over zeolites. The HPA catalysts reach ~100% *i*-PrOH conversion at 90 °C, whereas this occurs for zeolites at 140–180 °C. This can be explained by the stronger Brønsted acidity of HPA compared to zeolites [11–13] and the restricted accessibility of proton sites located in zeolite micropores. Also, zeolites, except for H-mordenite, exhibit a lower propene selectivity than the HPA/SiO₂ catalysts (cf. Figures 4 and 8).

The steeper increase in *i*-PrOH conversion with reaction temperature for HPA/SiO₂ compared to zeolites points to a higher activation energy of *i*-PrOH dehydration over HPA/SiO₂ compared to zeolites. The apparent activation energies E_a for zeolites and 25%HPA/SiO₂ were determined in the temperature range of 50–100 °C at *i*-PrOH conversion ≤10% for zeolites and ≤20% for 25%HPA/SiO₂. Arrhenius plots are shown in

Figure S1 in the Supplementary Materials. For zeolites, the E_a values were in the range from 98 to 121 kJ mol^{-1} (Table 3), with the lower E_a for the more active H-mordenite. Meanwhile, E_a values for 25%HPA/SiO₂ catalysts were 134–145 kJ mol^{-1} . Generally, E_a values for i-PrOH dehydration can vary over a wide range depending on the catalyst and reaction conditions [28]. Thus, the E_a values for $\gamma\text{-Al}_2\text{O}_3$, HY and 15%HPW/ZrO₂ have been reported to be 133–138 [29], 130 [30] and 100 kJ mol^{-1} [3], respectively.

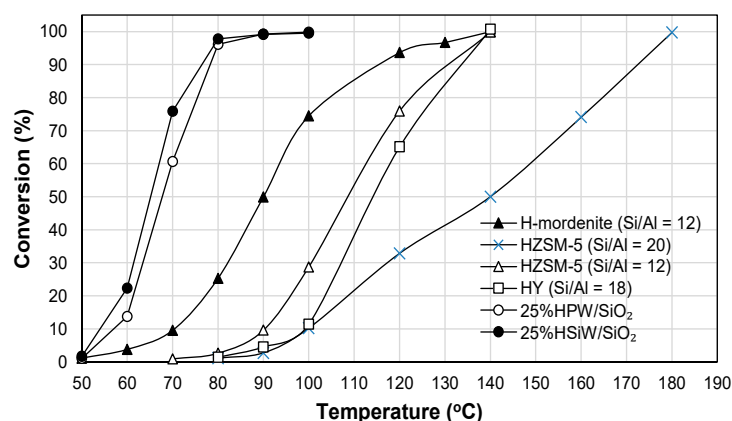


Figure 7. Effect of temperature on i-PrOH conversion over zeolite and 25%HPA/SiO₂ catalysts (0.20 g) at 20 mL min⁻¹ flow rate, 0.95 kPa i-PrOH partial pressure, $W/F = 422 \text{ g h mol}^{-1}$ and 2 h TOS.

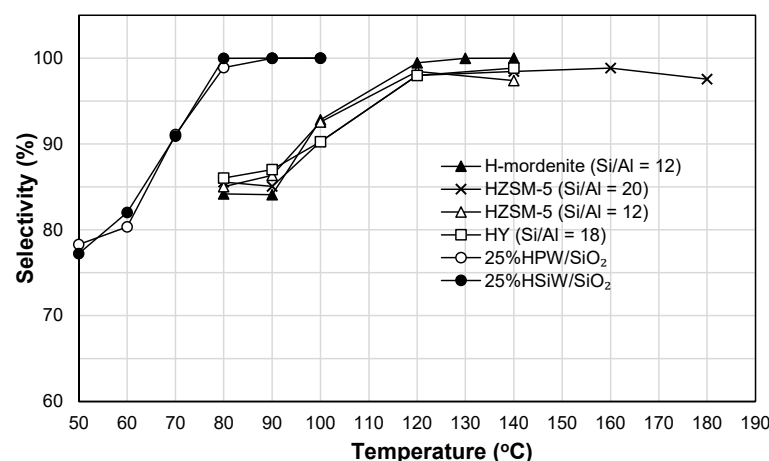


Figure 8. Effect of temperature on propene selectivity in i-PrOH dehydration over zeolite and 25%HPA/SiO₂ catalysts (0.20 g) at 20 mL min⁻¹ flow rate, 0.95 kPa i-PrOH partial pressure, $W/F = 422 \text{ g h mol}^{-1}$ and 2 h TOS.

Table 3. Apparent activation energies for i-PrOH dehydration over zeolites and 25%HPA/SiO₂.

Catalyst	E_a , kJ mol^{-1}
HZSM-5 (Si/Al = 12)	121
HZSM-5 (Si/Al = 20)	116
HY (Si/Al = 18)	114
H-mordenite (Si/Al = 12)	98
25%HPW/SiO ₂	134
25%HSiW/SiO ₂	145

2.2.3. Dehydration of i-PrOH Catalyzed by HPA/SiO₂: Effect of i-PrOH Partial Pressure

As i-PrOH dehydration is a zero-order reaction [4,6], increasing the partial pressure of i-PrOH is expected to decrease i-PrOH conversion. This is because the rate of a zero-order

reaction, approximated as $R = XF/W$ (X is the fractional conversion, F is the inlet molar flow rate of substrate and W is the catalyst weight) [31], does not depend on the partial pressure of substrate; hence, increasing the substrate partial pressure (i.e., increasing F) will cause a decrease in conversion X . In addition, an increase in *i*-PrOH partial pressure is expected to increase the selectivity to DIPE at the expense of propene. The results obtained showed that this was indeed the case (Table 4). For both 25%HSiW/SiO₂ and 25%HPW/SiO₂, the conversion almost halved as *i*-PrOH pressure was increased from 0.95 to 15 kPa at a constant temperature of 100 °C, with a simultaneous increase in DIPE selectivity at the expense of propene (the reaction time courses are shown in Figures S2 and S3).

Table 4. Effect of *i*-PrOH partial pressure on *i*-PrOH dehydration over 25%HPA/SiO₂ ^a.

Catalyst	Temperature °C	<i>i</i> -PrOH Pressure kPa	Conversion %	Selectivity, %	
				Propene	DIPE
25%HSiW/SiO ₂	100	0.95	99.5	100	0.0
	100	5.5	86.4	97.3	2.7
	100	10	69.4	94.5	5.5
	100	15	57.1	87.5	12.5
	120	15	97.2	99.4	0.6
	130	15	99.3	100	0
25%HPW/SiO ₂	100	0.95	99.5	100	0.0
	100	5.5	81.3	99.7	0.3
	100	10	66.0	95.8	4.2
	100	15	49.2	91.2	8.8
	120	15	96.2	99.1	0.9
	130	15	99.3	100	0

^a 0.20 g catalyst, 20 mL min⁻¹ N₂ flow rate, 2 h TOS.

Increasing the reaction temperature from 100 to 130 °C at 15 kPa *i*-PrOH pressure restored the conversion to >99% and propene selectivity to 100% (Table 4). Figure 9 shows the effect of reaction temperature in the range of 100–130 °C on the time course of *i*-PrOH dehydration at 15 kPa alcohol partial pressure for 25%HSiW/SiO₂. At 100 °C, an initial sharp decline in alcohol conversion was observed, with a stable *i*-PrOH conversion after that. The initial decline was probably due to the adsorption of by-product water blocking catalyst proton sites and reducing their strength. At higher temperatures of 120 and 130 °C, at which water adsorption should be weaker, stable conversion and product selectivity were observed from the beginning of reaction. Similar results were obtained for 25%HPW/SiO₂ (Figure S4).

2.2.4. Stability of Catalyst Performance

The performance stability of HPA/SiO₂ catalysts in *i*-PrOH dehydration was investigated at a relevant-to-practice *i*-PrOH partial pressure of 15 kPa and a temperature of 120 °C. The results are shown in Figure 10. As can be seen, there is no discernible catalyst deactivation over a TOS period of 24 h. The average *i*-PrOH conversion and propene selectivity were 97.1 and 99.4% for 25%HSiW/SiO₂ and 96.8 and 99.7% for 25%HPW/SiO₂, i.e., both catalysts exhibited very similar performance in *i*-PrOH-to-propene dehydration at ambient pressure. At 130 °C and 15 kPa *i*-PrOH partial pressure, both catalysts gave 100% propene selectivity at 99.3% *i*-PrOH conversion (Table 4).

It was also interesting to test the performance stability of zeolite catalysts under the same conditions for comparison with HPA/SiO₂. Figure 11 shows a 24 h stability test for the more active zeolite H-mordenite (Si/Al = 12). As can be seen, under the specified conditions, the zeolite not only gave significantly lower *i*-PrOH conversion and propene selectivity but also exhibited poor stability, with a decline in conversion from 47 to 22% over 24 h TOS. The lack of stability could be attributed to catalyst coking as well as capillary condensation of by-product water in zeolite pores at high *i*-PrOH partial pressures. This

demonstrates the great advantages of HPA catalysts over zeolites in *i*-PrOH-to-propene dehydration in terms of their activity, selectivity and mild operation conditions. It is noteworthy that these HPA catalysts are similar to those that are used in the industrial BP AVADA process for the synthesis of ethyl acetate [17–19].

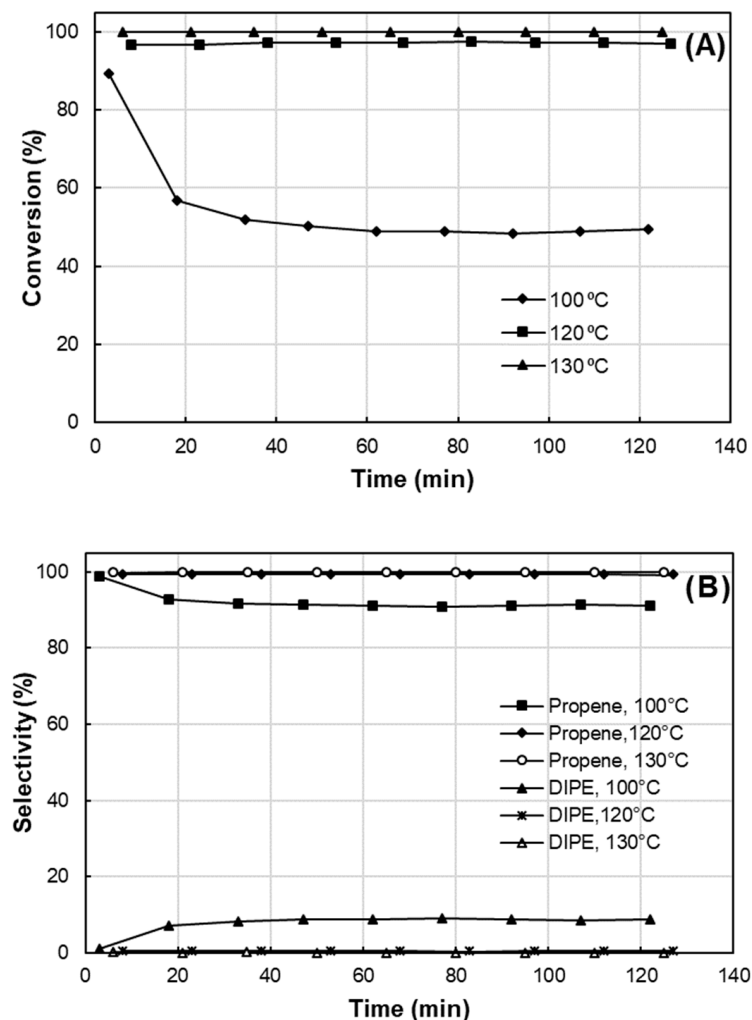


Figure 9. Effect of temperature on *i*-PrOH conversion (A) and product selectivity (B) over 25%HSiW/SiO₂ (0.20 g) at 20 mL min^{−1} flow rate, 15 kPa *i*-PrOH partial pressure, $W/F = 27 \text{ g h mol}^{-1}$ and 2 h TOS.

Finally, Table 5 shows the results of carbon analysis of spent 25%HPW/SiO₂ and 25%HSiW/SiO₂ catalysts after the reaction at 120 °C and 15 kPa *i*-PrOH partial pressure, carried out for 2 or 24 h TOS. As can be seen, the amount of carbon deposited on the catalysts was relatively small, at 1.8–2.5%, regardless of the reaction time. This suggests that coke mainly deposited in the beginning of the reaction, i.e., at TOS ≤ 2 h. The minor coking did not affect catalyst performance, as can be seen in Figure 10. The amount of coke deposited on H-mordenite (5.7%) was significantly larger (Table 5) and may have been responsible for the poor performance stability of this catalyst (Figure 11). For the deactivation of zeolite catalysts via coking, see [32].

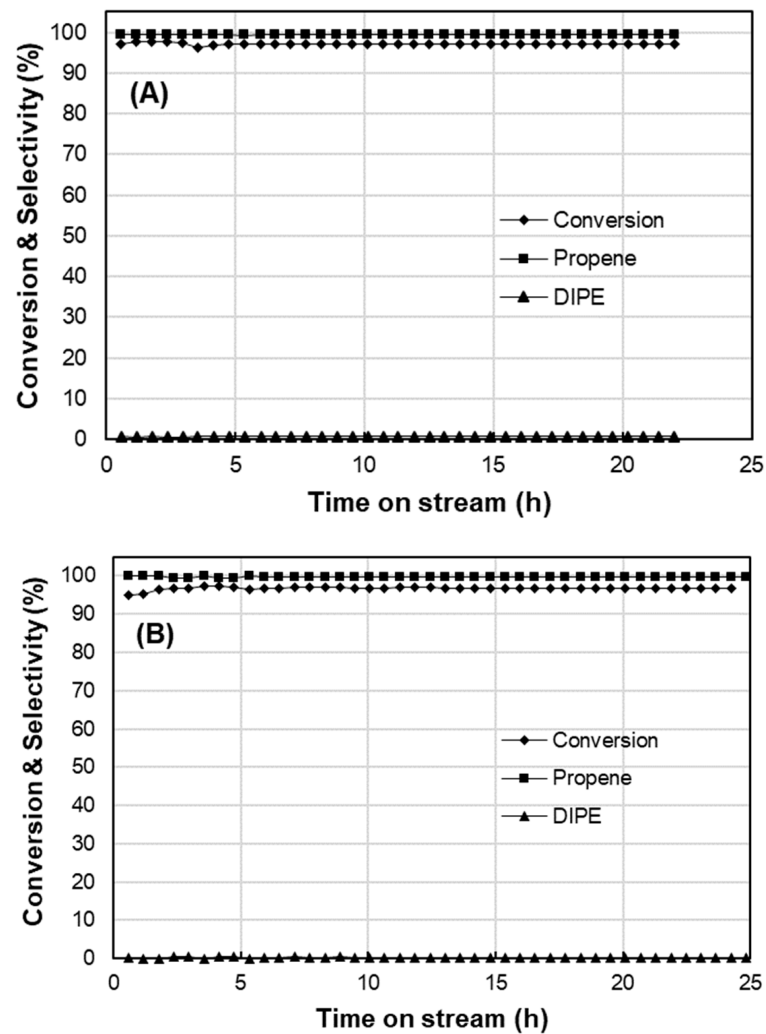


Figure 10. Time course for dehydration of *i*-PrOH over 25%HSiW/SiO₂ (A) and 25%HPW/SiO₂ (B) catalysts (0.20 g) at 120 °C, 20 mL min⁻¹ flow rate, 15 kPa *i*-PrOH partial pressure and $W/F = 27 \text{ g h mol}^{-1}$.

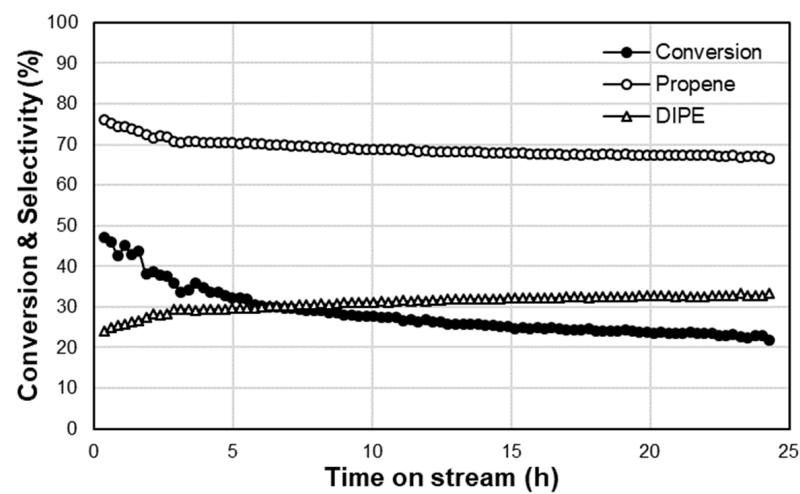


Figure 11. Time course for dehydration of *i*-PrOH over H-mordenite (Si/Al = 12) (0.20 g) at 120 °C, 20 mL min⁻¹ flow rate, 15 kPa *i*-PrOH partial pressure and $W/F = 27 \text{ g h mol}^{-1}$.

Table 5. Carbon content in spent 25%HPA/SiO₂ catalysts ^a.

Catalyst	Time on Stream, h	Carbon Content ^b , %
25%HPW/SiO ₂	24	1.8
25%HSiW/SiO ₂	24	2.2
25%HPW/SiO ₂	2	2.5
25%HSiW/SiO ₂	2	1.9
H-mordenite (Si/Al = 12)	24	5.7

^a Reaction conditions: 0.20 g catalyst, 120 °C, 15 kPa i-PrOH partial pressure, 20 mL min⁻¹ flow rate, W/F = 27 g h mol⁻¹. ^b From combustion chemical analysis.

3. Materials and Methods

3.1. Catalysts

H₃PW₁₂O₄₀ (99%) was acquired from Sigma–Aldrich (Gillingham, Dorset, UK) and H₄SiW₁₂O₄₀ (99.9%) from Fluka (Charlotte, NC, USA). From TGA analysis, HPW and HSiW contained 20–28 molecules of H₂O per HPA molecule (for the thermal dehydration of HPA, see [11,13,14]). i-PrOH (99.5%) was sourced from Sigma–Aldrich. Catalyst support Aerosil 300 silica was obtained from Degussa. Aluminosilicate zeolites H-mordenite (Si/Al = 12), HZSM-5 (Si/Al = 12), HZSM-5 (Si/Al = 20) and HY (Si/Al = 18) were procured from Zeolyst International (Conshohocken, PA, USA). Before use, the zeolites were calcined in air at 500 °C for 2 h.

Supported HPA catalysts HPA/SiO₂ (25 and 40% HPA content) were prepared as described elsewhere [20] via the wet impregnation of support with an aqueous solution of HPA. The catalysts were dried at 150 °C/1 Pa for 1.5 h and finally ground to a 45–180 µm particle size. HPA loading in the catalysts was determined by ICP-AES (inductively coupled plasma atomic emission spectroscopy) and water content by TGA.

3.2. Catalyst Characterization

The texture of catalysts (surface area and porosity) was characterized using the BET method on a Micromeritics 3Flex instrument (Micromeritics Instrument Corp., Norcross, GA, USA). Before analysis, the catalysts were heated at 220 °C for 1 h in a vacuum. Thermogravimetric analysis (TGA) was carried out on a TA TGA 55 thermal analyzer (TA Instruments, USA) under N₂ atmosphere. X-ray diffraction (XRD) patterns of catalysts were obtained on a PANalytical Xpert diffractometer (Malvern Panalytical, Malvern, UK) with CuKα radiation (λ = 1.542 Å). DRIFT (diffuse reflectance infrared Fourier transform) spectra were recorded on a Nicolet Nexus FTIR spectrometer (Nicolet Instrument Corp., Madison, WI, USA) using powdered catalyst mixtures with KBr. The same instrument was used for recording DRIFT spectra of adsorbed pyridine (Py-DRIFTS), as described previously [3]. The ICP–OES analysis of catalysts was performed on a Spectro Ciros ICP–OES instrument (Spectro Analytical Instruments GmbH, Kleve, Germany); catalyst samples were digested by boiling in 15% aqueous KOH.

3.3. Catalyst Testing

The dehydration of i-PrOH was carried out at 50–130 °C, under ambient pressure in a Pyrex fixed-bed microreactor (9 mm i.d.) with online GC analysis (Agilent 8860 GC System, flame ionization detector, 30 m × 0.32 mm × 0.5 µm Agilent CP-WAX 52 CB capillary column), as described elsewhere [4]. i-PrOH was fed with flowing nitrogen (20 mL min⁻¹) through a saturator holding i-PrOH at 0, 25, 33.6 and 41.1 °C to maintain the chosen alcohol partial pressures of 0.95, 5.52, 10 and 15 kPa, respectively [33]. The catalysts were pretreated at the reaction temperature in N₂ flow for 1 h. The mean absolute percentage error in i-PrOH conversion was ≤5% and the carbon balance was maintained within 95%. The rate of reaction (*R*, mol g⁻¹ h⁻¹) was calculated as $R = XF/W$, where *X* is i-PrOH conversion,

W/F is the contact time (g h mol^{-1}), W is the catalyst weight and F is the inlet molar flow rate of *i*-PrOH [31].

4. Conclusions

This work has demonstrated excellent performance of silica-supported Keggin-type heteropoly acids HPW and HSiW for gas-phase *i*-PrOH-to-propene dehydration at relevant-to-practice *i*-PrOH partial pressures and ambient total pressure. These catalysts show similar efficacies, giving an *i*-PrOH conversion and propene selectivity of 96.8 and 99.7% for 25%HPW/SiO₂ and 97.1 and 99.4% for 25%HSiW/SiO₂ at 120 °C, 15 kPa *i*-PrOH partial pressure and a contact time $W/F = 27 \text{ g h mol}^{-1}$ (GHSV = 900 mL g⁻¹ h⁻¹) in a fixed-bed reactor, without any catalyst deactivation for at least 24 h time on stream. The HPA catalysts are superior to aluminosilicate zeolites such as H-mordenite, HZSM-5 and HY in terms of *i*-PrOH conversion, propene selectivity and catalyst stability and, therefore, have great potential as catalysts for the production of propene via *i*-PrOH dehydration at ambient pressure.

Supplementary Materials: The following supporting information can be downloaded at: <https://www.mdpi.com/article/10.3390/catal14010051/s1>, Figure S1: Arrhenius plots for *i*-PrOH dehydration over zeolites and 25%HPA/SiO₂ catalyst; Figure S2: Effect of *i*-PrOH partial pressure on *i*-PrOH conversion and product selectivity over 25%HPW/SiO₂ catalyst; Figure S3: Effect of *i*-PrOH partial pressure on *i*-PrOH conversion and product selectivity over 25%HSiW/SiO₂ catalyst; Figure S4: Effect of temperature on *i*-PrOH conversion and product selectivity over 25%HPW/SiO₂ catalyst.

Author Contributions: Conceptualization, I.V.K.; methodology, I.V.K. and E.F.K.; investigation and data curation, A.A.; writing—original draft preparation, A.A.; writing—review and editing, I.V.K.; supervision, I.V.K. and E.F.K. All authors have read and agreed to the published version of the manuscript.

Funding: This research received no external funding.

Data Availability Statement: The data presented in this study are openly available.

Acknowledgments: We thank King Khalid University for its PhD scholarship for Amal Alasmari.

Conflicts of Interest: The authors declare no conflicts of interest.

References

1. Hattori, H.; Ono, Y. *Solid Acid Catalysis. From Fundamentals to Applications*; CRC Press: Boca Raton, FL, USA, 2015.
2. Macht, J.; Janik, M.; Neurock, M.; Iglesia, E. Mechanistic consequences of composition in acid catalysis by polyoxometalate Keggin clusters. *J. Am. Chem. Soc.* **2008**, *130*, 10369–10379. [[CrossRef](#)] [[PubMed](#)]
3. Alsalmeh, A.M.; Wiper, P.V.; Khimiyak, Y.Z.; Kozhevnikova, E.F.; Kozhevnikov, I.V. Solid acid catalysts based on H₃PW₁₂O₄₀ heteropoly acid: Acid and catalytic properties at a gas-solid interface. *J. Catal.* **2010**, *276*, 181–189. [[CrossRef](#)]
4. Bond, G.C.; Frodsham, S.J.; Jubb, P.; Kozhevnikova, E.F.; Kozhevnikov, I.V. Compensation effect in isopropanol dehydration over heteropoly acid catalysts at a gas-solid interface. *J. Catal.* **2012**, *293*, 158–164. [[CrossRef](#)]
5. Alasmari, A.; Al-Faze, R.; Kozhevnikova, E.F.; Kozhevnikov, I.V. Solid acid catalysts comprising heteropoly acids supported on SiO₂, TiO₂ and ZrO₂: A microcalorimetric investigation of catalyst acidity and new insight into the mechanism of alcohol dehydration over HPA. *Catal. Commun.* **2023**, *180*, 106710. [[CrossRef](#)]
6. Gervasini, A.; Fenyvesi, J.; Auroux, A. Study of the acidic character of modified metal oxide surfaces using the test of isopropanol decomposition. *Catal. Lett.* **1997**, *43*, 219–228. [[CrossRef](#)]
7. Weissmehl, K.; Arpe, H.J. *Industrial Organic Chemistry*, 4th ed.; Wiley-VCH: Weinheim, Germany, 2003.
8. Dubois, J.L.; Postole, G.; Silvester, L.; Auroux, A. Catalytic dehydration of isopropanol to propylene. *J. Catal.* **2022**, *12*, 1097. [[CrossRef](#)]
9. Liew, F.E.; Nogle, R.; Abdalla, T.; Rasor, B.J.; Canter, C.; Jensen, R.O.; Wang, L.; Strutz, J.; Chirania, P.; De Tissera, S.; et al. Carbon-negative production of acetone and isopropanol by gas fermentation at industrial pilot scale. *Nat. Biotechnol.* **2022**, *40*, 335–344. [[CrossRef](#)]
10. Klabunde, J.; Bischoff, C.; Papa, A.J. Propanols. In *Ullmann's Encyclopedia of Industrial Chemistry*; Wiley-VCH: Weinheim, Germany, 2018.
11. Okuhara, T.; Mizuno, N.; Misono, M. Catalytic chemistry of heteropoly compounds. *Adv. Catal.* **1996**, *41*, 113–252.
12. Mizuno, N.; Misono, M. Heterogeneous catalysis. *Chem. Rev.* **1998**, *98*, 199–217. [[CrossRef](#)]

13. Kozhevnikov, I.V. Catalysis by Polyoxometalates. In *Catalysts for Fine Chemicals*; Wiley: Chichester, UK, 2002; Volume 2.
14. Moffat, J.B. *Metal-Oxygen Clusters. The Surface and Catalytic Properties of Heteropoly Oxometalates*; Kluwer: New York, NY, USA, 2001.
15. Misono, M. *Heterogeneous Catalysis of Mixed Oxides. Perovskite and Heteropoly Catalysts*; Elsevier: Amsterdam, The Netherlands, 2013.
16. Misono, M. A view on the future of mixed oxide catalysts: The case of heteropolyacids (polyoxometalates) and perovskites. *Catal. Today* **2005**, *100*, 95–100. [[CrossRef](#)]
17. Dobson, I.D. Leaps of innovation. *Green Chem.* **2003**, *5*, G78–G81.
18. Van Wettere, B.; Aghakhani, S.; Lauwaert, J.; Thybaut, J.W. Ethyl acetate synthesis by direct addition of acetic acid to ethylene on a silicotungstic acid catalyst: Experimental assessment of the kinetics. *Appl. Catal.* **2022**, *646*, 118849. [[CrossRef](#)]
19. Ethanol to Ethylene Conversion, Hummingbird Technology. Available online: <https://www.bio.org/sites/default/files/1500%20Langston.pdf> (accessed on 3 January 2024).
20. Al-Faze, R.; Finch, A.; Kozhevnikova, E.F.; Kozhevnikov, I.V. Dehydration of methanol and ethanol over silica-supported heteropoly acids in the gas phase: Surface-type versus bulk-type catalysis mechanism. *Appl. Catal.* **2020**, *597*, 117549. [[CrossRef](#)]
21. Rocchiccioli-Deltcheff, C.; Fournier, M.; Franck, R.; Thouvenot, R. Vibrational investigations of polyoxometalates: Evidence for anion-anion interactions in molybdenum(VI) and tungsten(VI) compounds related to the Keggin structure. *Inorg. Chem.* **1983**, *22*, 207–216. [[CrossRef](#)]
22. Knözinger, H. Infrared spectroscopy for the characterization of surface acidity and basicity. In *Handbook of Heterogeneous Catalysis*, 2nd ed.; Ertl, G., Knözinger, H., Schüth, F., Weitkamp, J., Eds.; Wiley-VCH: Weinheim, Germany, 2008; Volume 2, p. 1138.
23. Bardin, B.B.; Bordawekar, S.V.; Neurock, M.; Davis, R.J. Acidity of Keggin-type heteropolycompounds evaluated by catalytic probe reactions, sorption microcalorimetry, and density functional quantum chemical calculations. *J. Phys. Chem. B* **1998**, *102*, 10817–10825. [[CrossRef](#)]
24. Kapustin, G.I.; Brueva, T.R.; Klyachko, A.L.; Timofeeva, M.N.; Kulikov, S.M.; Kozhevnikov, I.V. A study of the acidity of heteropoly acids. *Kinet. Katal.* **1990**, *31*, 1017–1020.
25. Newman, A.D.; Brown, D.R.; Siril, P.; Lee, A.F.; Wilson, K. Structural studies of high dispersion H₃PW₁₂O₄₀/SiO₂ solid acid catalysts. *Phys. Chem. Chem. Phys.* **2006**, *8*, 2893–2902. [[CrossRef](#)]
26. Alharbi, W.; Kozhevnikova, E.F.; Kozhevnikov, I.V. Dehydration of MeOH to dimethyl ether over heteropoly acid catalysts: The relationship between reaction rate and catalyst acid strength. *ACS Catal.* **2015**, *5*, 7186–7193. [[CrossRef](#)]
27. Brandle, M.; Sauer, J. Acidity differences between inorganic solids induced by their framework structure. a combined quantum mechanics/molecular mechanics ab initio study on zeolites. *J. Am. Chem. Soc.* **1998**, *120*, 1556–1570. [[CrossRef](#)]
28. Ghosh, A.; Bhaduri, K.; Shaha, S.; Auroux, A.; Pandey, J.K.; Chowdhury, B. Dehydration of isopropanol to propylene over fullerene[C₆₀] containing niobium phosphate catalyst: Study on catalyst recyclability. *Molec. Catal.* **2019**, *475*, 110470. [[CrossRef](#)]
29. Larmier, K.; Chizallet, C.; Cadran, N.; Maury, S.; Abboud, J.; Lamic-Humblot, A.-F.; Marceau, E.; Lauron-Pernot, H. Mechanistic investigation of isopropanol conversion on alumina catalysts: Location of active sites for alkene/ether production. *ACS Catal.* **2015**, *5*, 4423–4437. [[CrossRef](#)]
30. Murphy, B.M.; Wu, J.; Cho, H.J.; Soreo, J.; Wang, C.; Ma, L.; Xu, B. Nature and catalytic properties of in-situ-generated Brønsted acid sites on NaY. *ACS Catal.* **2019**, *9*, 1931–1942. [[CrossRef](#)]
31. Kapteijn, F.; Marin, G.B.; Moulijn, J.A. Catalytic Reaction Engineering. In *Catalysis: An Integrated Approach*, 2nd ed.; van Santen, R.A., van Leeuwen, P.W.N.M., Eds.; Elsevier: Amsterdam, The Netherlands, 2000; pp. 375–430.
32. Derouane, E.G. Factors affecting the deactivation of zeolites by coking. *Stud. Surf. Sci. Catal.* **1985**, *20*, 221–240.
33. CRC. *Handbook of Chemistry and Physics*, 103rd ed.; Rumble, J.R., Ed.; CRC Press: Boca Raton, FL, USA, 2023.

Disclaimer/Publisher's Note: The statements, opinions and data contained in all publications are solely those of the individual author(s) and contributor(s) and not of MDPI and/or the editor(s). MDPI and/or the editor(s) disclaim responsibility for any injury to people or property resulting from any ideas, methods, instructions or products referred to in the content.